Cell Biology of Pathologic Renal Calcification: Contribution of Crystal Transcytosis, Cell-Mediated Calcification, and Nanoparticles

Vivek Kumar, Gerard Farell, Shihui Yu, Sean Harrington, Lorraine Fitzpatrick, Ewa Rzewuska, Virginia M. Miller, and John C. Lieske

Introduction: The earliest lesion in the kidneys of idiopathic calcium oxalate stone formers is deposition of calcium phosphate in the interstitium, termed a Randall's plaque. Yet the cellular and molecular factors leading to their formation are unknown.

Methods: The influence of urinary proteins on adhesion of preformed calcium oxalate crystals to rat continuous inner medullary collecting duct (cIMCD) cells was studied in vitro, and cIMCD cells were also exposed to calcifying media containing β-glycerophosphate for up to 28 days. Renal tissue was obtained from a stone-forming and non–stone-forming individual at the time of nephrectomy. These nanoparticles, isolated from renal stones obtained at the time of surgical resection, were analyzed and propagated in standard cell culture medium.

Results: Urinary proteins influence crystal adhesion to renal epithelial cells, and this activity is abnormal in the urine of stone-forming patients. cIMCD cells assumed an osteoblastic phenotype when exposed to the calcifying medium, expressing two bone matrix proteins (osteopontin and bone sialoprotein) that were also identified in the kidney of the stone-forming patient and associated with crystal deposition. Nanoparticles were propagated from the majority of renal stones. Isolates were susceptible to selected metabolic inhibitors and antibiotics and contained conserved bacterial proteins and deoxyribonucleic acid (DNA).

Conclusions: These results suggest new paradigms for Randall's plaque formation and idiopathic calcium oxalate stone disease. It seems unlikely that these events are driven solely by physical chemistry; rather, they are critically influenced by specific proteins and cellular responses, and understanding these events will provide clues toward novel therapeutic targets.

Key words: bone sialoprotein, continuous inner medullary collecting duct cells, nanobacteria, nephrolithiasis, osteopontin

From the Division of Nephrology (V.K., G.F., S.Y., J.C.L.), Division of Endocrinology (S.H., L.F.), and Departments of Surgery and Physiology and Biomedical Engineering (E.R., V.M.M.), Mayo Clinic College of Medicine, Rochester, MN.

This work was supported by grants from the National Institutes of Health (DK 53399, DK 60707, and DK 62021), The Ralph C. Wilson, Sr., and Ralph C. Wilson, Jr. Medical Research Foundation, the Oxalosis and Hyperoxaluria Foundation, and the Mayo Foundation.

Presented at Experimental Biology 2006, San Francisco, CA, April 1–5, 2006.

Address correspondence to: Dr. John C. Lieske, Division of Nephrology, Mayo Clinic College of Medicine, 200 First Street SW, Rochester, MN 55905; e-mail: Lieske.John@mayo.edu.

Journal of Investigative Medicine 2006; 54:412–424.

DOI 10.2310/6650.2006.06021

The formation of kidney stones affects 12% of men and 5% of women in industrialized countries by age 70 years,[1] including 900,000 persons in the United States each year.[2] However, the mechanisms by which renal calculi arise are poorly understood. Although renal tubular fluid and final urine are often supersaturated with calcium, phosphate, and oxalate ions, mechanisms whereby calcium oxalate and calcium phosphate crystals are retained in the kidney are largely unknown, and the underlying cell biology of renal stone initiation and propagation remains enigmatic. In this article, we review the potential mechanisms for the formation of Randall's plaques, an apparent critical precursor of idiopathic calcium oxalate stones.

Randall's Plaques

In the 1930s, Alexander Randall first described the calcified plaques, which now bear his name, buried beneath the epithelium of cadaveric renal papillae.[3,4]

He theorized that these plaques became the nidus for renal stone formation if they lost their epithelial covering and became bathed in calyceal urine, allowing urinary salts to crystallize on the plaque like a foreign body. He observed plaques in approximately 20% of the 1,154 kidney pairs he examined. In addition, Randall described papillary calculi as characteristically having a smooth convex surface and a concave surface, which he believed to be the site of papillary implantation. In the 1980s, Cifuentes Delatte and colleagues examined 500 spontaneously passed renal calculi and found 28% to demonstrate morphology consistent with a papillary implantation site.[5] Most commonly, the implantation site was composed of calcium phosphate, with the stone itself composed of calcium oxalate.

Stoller and colleagues used high-resolution radiography to examine 50 consecutive sets of cadaveric kidneys.[6] Renal medullary calcifications that extended deep into the papillae were identified in 57%. When histologically examined, the calcification was localized to the basement membrane of collecting tubules and vasa recta, as well as within the papillary interstitium. Of the limited available clinical data, only a history of hypertension appeared to correlate with an increased incidence of calcifications. In the kidneys of patients undergoing percutaneous or ureteroscopic stone extraction, Low and Stoller commonly observed subendothelial plaques.[7] Plaques were found in 87% of calcium oxalate ($n = 25$) and 100% of calcium phosphate stone formers ($n = 12$) versus only 43% of patients having procedures for nonstone reasons ($n = 7$). Plaques were also common in uric acid stone formers (100%, $n = 3$) but relatively less common among struvite (2 of 10) or cystine (2 of 6) stone formers.

The histopathology of Randall's plaques has been redefined in detail.[8] Intraoperative biopsies were obtained in 15 persons with calcium oxalate stone disease and compared with those of 4 persons without nephrolithiasis. Endoscopically, Randall's plaques were identified in all 15 patients with calcium oxalate stones. Microscopically, deposits were located in the interstitial spaces and followed bundles of the thin loops of Henle and vasa recta up to the inner medulla. Interstitial deposits ranged from single spheres, as small as 50 nm, to large, dense collections. In certain regions, the crystal deposition was more dense, entirely surrounding loops of Henle (or more rarely collecting ducts), appearing with cells that demonstrated vacuolization and detachment from the basement membrane. The smallest and presumably initial deposits appeared to arise in the basement membrane of the thin limb of the loop of Henle. Crystallographically, the deposits were composed of hydroxyapatite. In the nonstone formers, no gross Randall's plaques were observed, and only a few small deposits near loops of Henle were observed in two of the four kidneys studied.

Therefore, interstitial calcium phosphate deposits appear to be present within the kidney of most ''idiopathic'' calcium oxalate stone formers, and in their final stage, these deposits coalesce to form Randall's plaques. The pathology has been interpreted to suggest that the earliest deposits arise near the thin limbs of the loop of Henle and in the basement membrane surrounding the vasa recta.[8] However, the pathways by which these calcium phosphate deposits arise, the apparent precursor of stones, remain unclear. Could Randall's plaques be the end result of transcytosis of newly formed crystals from the interstitium? Could they nucleate directly in the interstitium, perhaps driven by cell-mediated pathways? Could they result from colonization with a novel, calcifying entity (nanobacteria)? We review evidence to support all three possibilities, which are not necessarily mutually exclusive.

Could Randall's Plaques Arise from Tubular Fluid?

Crystals are often found in the urine, more commonly in those who form stones,[9] in part because stone formers tend to have higher prevailing supersaturations with respect to calcium oxalate and calcium phosphate. In addition, evidence also suggests that stone-former urine often behaves differently and decreases crystallization processes less than non–stone former urine.[10,11] Many of the macromolecules that can be isolated from urine and inhibit crystallization appear to be polyanionic in the size range of 14 to 200 kDa.[12] Once crystals nucleate and grow within tubular fluid, the next critical factor could be their adhesion to epithelial cells, allowing their retention within the kidney. Further, cultured renal cells can bind and internalize CaOx and CaP crystals, which are subsequently dissolved within lysosomes.[13,14] Soluble urinary proteins also appear to regulate this process because they can block crystal binding to cells.[15] Incorporation of proteins into crystals also appears to hasten their dissolution within cells.[16] Therefore, evidence suggests that macromolecules in urine can block crystal formation and retention within the kidney via multiple potential pathways.

Which of the urinary proteins are most critical for regulating crystallization? Overall, current evidence is strongest for Tamm-Horsfall protein (THP),[17–19]

osteopontin (OPN),[20] bikunin,[21] and urinary prothrombin fragment 1 (UPTF1).[22] Although all four proteins are present and active when studied in vitro, none appear to be quantitatively reduced in the urine of the majority of stone formers. However, data do suggest functional alterations in THP isolated from the urine of nephrolithiasis patients,[23–26] perhaps owing to abnormal glycosylation. Further, differences between UPTF1 activity in the urine of blacks and whites in South Africa have been suggested as a reason for differences in stone risk between the two populations.[27] A study from our laboratory also suggests that THP may differ functionally between stone formers and controls.[28] Total urinary protein in a group of stone-forming men blocked crystal adhesion to renal cells less than urinary proteins from matched controls. When incubated with calcium oxalate monohydrate (COM) crystals, association of UPTF1, OPN, and bikunin with the crystals did not differ between stone formers and controls. However, THP in stone-former urine was functionally abnormal and did not coat crystals.[28] Earlier studies also suggested a dysfunctional THP in a small group of recurrent stone formers in whom the glycoprotein demonstrated an increased tendency to self-aggregate[23] and had an abnormal charge,[25,26] perhaps owing to decreased sialic acid content.[24] A mouse knockout model confirms the in vivo anticrystallization activity of THP[29] and OPN.[30] Functional changes in THP could be acquired, rather than or in addition to being genetically mediated, because THP from the urine of hyperoxaluric stone formers and hypertensive individuals had reduced sialic acid content and promoted formation of COM crystal aggregates, and these properties of THP were partially reversed with oral vitamin E.[31]

Evidence suggests that CaOx and CaP crystals can bind to anionic structures on the surface of renal epithelial cells in culture,[14,32] including phosphatidylserine,[33] OPN,[34] nucleolin-related protein,[35] hyaluronan,[36] and annexin II.[37] Given that phosphatidylserine is present on the apical surface only when cells are apoptotic[33] and hyaluronan is apically expressed only when renal cells are proliferating in response to injury,[36] a popular hypothesis is that injury stimulates apical expression of receptor molecules, leading to increased retention of crystals. Potential injurious stimuli include oxalate ions or ischemia.[38]

Adhesion of CaOx crystals from nephron fluid to renal cells may be particularly important in states of marked hyperoxaluria, such as primary or enteric hyperoxaluria, where intratubular, intracellular, and interstitial CaOx crystals are commonly seen, associated with cellular reactions.[8,39–44] Recent evidence that calcium phosphate crystal–cell interactions also occur in vivo was supplied by the pathologic description of the renal failure and nephrocalcinosis that can occur after oral sodium phosphate bowel cleansing.[45] Intraluminal and intracellular calcification was observed early after exposure to the phosphate load (days to weeks), followed by interstitial crystalline deposits and fibrosis months to years later. These cases represent an extreme case associated with marked CaP crystalluria, whereas primary and enteric hyperoxaluria might represent an analogous extreme outcome of CaOx crystalluria. Other examples of nephrocalcinosis (Dent's disease,[46] renal allograft, and neonatal nephrocalcinosis[47]) could be examples in which increased expression of cell surface receptors promotes nephrocalcinosis. In this paradigm of crystal retention, renal calcification might result when modest intermittent crystalluria combines with sufficient expression of cell surface receptors, and clinical nephrolithiasis could occur when the number of retained crystals exceeds the ability of renal processing mechanisms.

Could Crystals Arise Directly in the Interstitium?

Over recent years, numerous groups have investigated the calcification processes that occur in human vasculature.[48] Bone-associated proteins, including OPN, bone morphogenetic protein 2, alkaline phosphatase, matrix Gla protein, osteocalcin, bone sialoprotien (BSP), and type I collagen, have all been detected,[49–52] suggesting that vascular smooth muscle cells can be induced to promote calcification and behave analogously to osteoblasts. We recently hypothesized that human renal cells might behave analogously to vascular smooth muscles in culture and that interstitial calcification could be driven by cellular events rather than by passive accumulation of mineral. To provide support for this hypothesis, continuous inner medullary collecting duct (cIMCD) cells[53] were grown under standard conditions used to induce osteoblastic phenotypic differentiation of vascular smooth muscle cells.[54] Culture media was replaced after 24 hours with nodule-inducing media: Dulbecco's Modified Eagle Medium (DMEM) plus 5% fetal calf serum (FCS) plus 10^{-8} M dexamethasone. After 48 hours of pretreatment, the nodule-inducing medium was replaced with calcification medium: DMEM plus 1% FCS plus 10 mM β-glycerophosphate disodium salt (BGP, Sigma G-9891, St. Louis, MO) plus 100 μM (18 μg/mL) L-ascorbic acid and a final calcium concentration of 2.5 mM calcium chloride because initial pilot studies defined a calcium concentration of 2.5 mM as optimal. Calcification media was

replaced every 2 to 3 days for up to 28 days. To quantitate monolayer-associated calcium, cells were washed extensively with saline G (NaCl 8.0 g/L, KCl 0.4 g/L, KH_2PO_4 0.15 g/L, Na_2HPO_4 0.29 g/L, $MgSO_4$ 0.154 g/L, and $CaCl_2$ 0.0147 g/L) and incubated with lysis buffer (0.6N HCl in 0.02 M phosphate-buffered saline) for 24 hours at 23°C, and the calcium in the supernatant was measured by optical emission spectroscopy in the Mayo Clinic Metals Laboratory.[54] When grown in calcifying media containing BGP, cIMCD cells demonstrated progressive nodule formation, with concurrent increases in cell-associated calcium at 4 weeks of 24% relative to control cells grown in standard DMEM. The nodules that formed stained with von Kossa's stain, indicating the presence of associated calcium (Figure 1). Antibodies against two bone matrix proteins, OPN and BSP, stained regions within nodules (see Figure 1), suggesting that these proteins could regulate calcification, with BSP promoting and OPN inhibiting calcium deposition in a negative feedback response.

To obtain evidence of similar findings in vivo, renal medullary tissue was obtained from uninvolved portions of a kidney removed from a 65-year-old calcium oxalate stone-forming woman because it contained a renal cell cancer. Calcification was observed in the medullary interstitium, as well as within tubules, when representative sections were stained by the von Kossa method. Both OPN and BSP immunostaining were detected in association with microcrystals, as well as within nearby cells and matrix, suggesting that these proteins are present in the intact kidney during crystal deposition. Neither protein was reliably detected in the kidney obtained from the non–stone former.

These preliminary data support the hypothesis that renal cells in culture can assume an osteoblast-like phenotype, express the matrix proteins OPN and BSP, and form calcified nodules. These results provide support for the hypothesis that renal cells may promote the formation of Randall's plaques, perhaps via expression of matrix proteins.

Could Nanoparticles Be the Cause of Randall's Plaques?

Nanobacteria were initially isolated from calf serum used for tissue culture experiments.[55] The term *nanoparticles* is now used by convention because there is no compelling evidence yet that they are, in fact, true bacterium. Conditions to culture nanoparticles are unusual because their growth rate is only one one-hundredth that of other bacteria and requires several weeks in tissue culture medium; gamma irradiation of the serum prevents their growth.[56] Perhaps their most striking feature is a thick calcium phosphate shell that surrounds these ≈100 nm–sized particles.[56] In addition to calf serum, nanoparticles have been isolated from human serum, urine, kidney stones, and renal cyst fluid obtained from patients with autosomal dominant polycystic kidney disease.[55,57–59] Nanoparticles appear to be susceptible to antibiotics, including tetracycline (TCN), trimethoprim-sulfamethoxazole, nitrofurantoin, and ampicillin,[60] but resistant to erythromycin, ciprofloxacin, rifampin, and penicillin. An independent group published the results of experiments in which calcifying nanoparticles were propagated from human kidney stones.[61] When the calcium shell dissolved, these nanoparticles contained a distinct array of proteins when resolved by sodium dodecyl sulfate–polyacrylamide gel electrophoresis (SDS PAGE). A polyclonal antibody raised against a nanoparticle lysate of bovine origin recognized a prominent 39 kDa band.

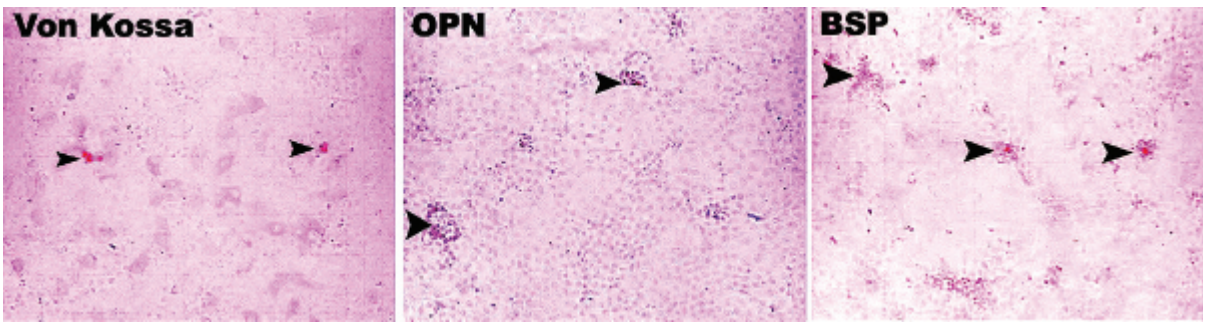

Figure 1 Formation of calcifying nodules by cultured continuous inner medullary collecting duct (cIMCD) renal epithelial cells. cIMCD cells were grown to confluence and exposed to calcifying media. Nodules were apparent by 7 days and more pronounced by 14 days. Positive staining for calcium by von Kossa's stain was apparent in the nodules, which also stained for the bone matrix proteins osteopontin (OPN) and bone sialoprotein (BSP) (*brown*). Staining with preimmune immunoglobulin G (control) was negative, supporting the specificity of the reaction (×100 original magnification).

Demineralized nanobacteria stained with propidium iodide, consistent with the present of deoxyribonucleic acid (DNA). Controversy remains, however, as these organisms have been difficult for many groups to culture. Cisar and colleagues successfully propagated organisms that possessed the physical characteristics of putative nanobacteria from saliva[62] but were unable to detect novel DNA in their cultures. Therefore, they concluded that their ''nanobacteria'' represented a form of biomineralization initiated by nonliving macromolecules, perhaps similar to matrix vesicles.[63]

It is notable that the early microcalcifications of Randall's plaque described by Evan and colleagues[8] are of a size and morphology similar to those of the nanoparticles we and others observed in human tissues[64] and cultured from diseased aortas and human renal stones. Although it is assumed that the unique ionic milieu in the medulla near the loop of Henle promotes the growth of these calcium phosphate deposits via physicochemical mechanisms, is it possible that this same milieu may be ideal for the growth of nanoparticles and that perhaps they preferentially colonize there.

To define the nature of nanoparticles and their potential relationship to Randall's plaques, at the Mayo Clinic, two well-characterized ''standard'' strains of nanoparticles isolated from bovine serum, ''S90'' and ''NBCS'', were obtained from Dr. Kajander and subcultured in 10 mL tissue culture flasks at 37°C in a CO_2 incubator in DMEM without calf serum to avoid this potential source of contaminating organisms, protein, and/or lipids. After several weeks, the growth of apparently motile particles less than a micron in size was observed by phase-contrast microscopy. Every 4 to 6 weeks, the flasks were scraped with a rubber spatula and divided 1:10 into fresh DMEM for subculture. These forms were characterized after centrifugation to form a pellet (150,000*g* for 40 minutes). By transmission electron microscopy (TEM), 50 to 100 nm–sized structures were observed that appeared to contain an inner core surrounded by a calcified shell (Figure 2A). These structures were similar to those observed by Kajander and Ciftcioglu.[65] Uninnoculated control flasks with media alone did not demonstrate growth of particulates. Energy-dispersive microanalysis confirmed that the shell was calcium phosphate. The calcium phosphate shell was next dissolved to visualize what was underneath. A pelleted sample was treated with ethylenediaminetetraacetic acid (EDTA) (0.3 mM at 4°C overnight), centrifuged, and prepared for TEM. Membranous structures 50 to 100 nm in size were observed (arrow, Figure 2B), which matched in appearance and size the inner cores seen in the calcified sample (see asterisk, Figure 2A).

To measure any nucleic acids that might be present, four additional flasks of nanoparticles were decalcified. Using quantitation kits from Molecular Probes (Carlsbad, CA), 0.9 μg of double-stranded DNA (PicoGreen) and 16.2 μg of ribonucleic acid (RNA) (RiboGreen) were detected. This DNA to RNA ratio is similar to that found in other prokaryotes, and the total quantity of each corresponds roughly to that of 10^8 *Escherichia coli* cells. As a negative control, DMEM with and without calf serum and/or calcium phosphate crystals were all processed similarly. Neither DNA nor RNA was detected in these negative controls.

To quantitatively evaluate the effects of various agents on nanoparticle growth, an assay in 96-well

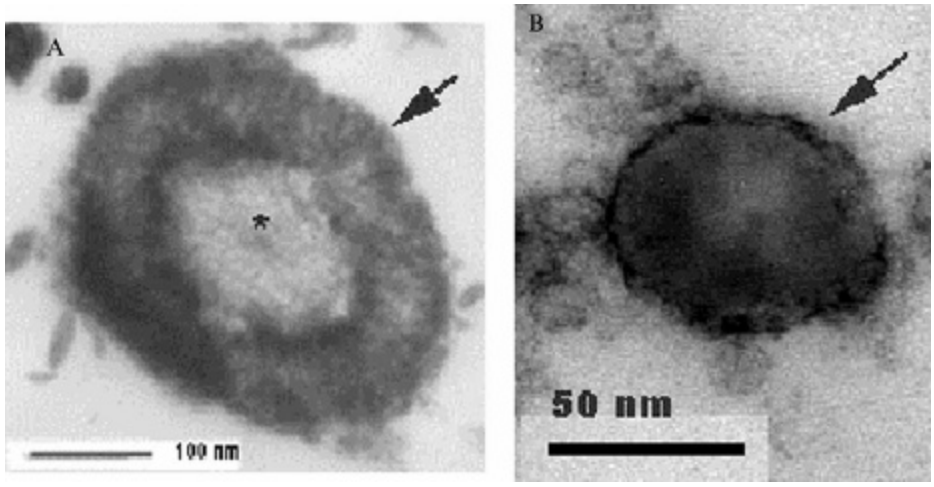

Figure 2 Nanoparticles (NBCS strain) by transmission electron microscopy. *A*, Calcified sample. Inner core (*asterisk*) and outer calcium phosphate shell (*arrow*) are seen. *B*, Decalcified sample. Membranous structures are seen (*arrow*).

plates was developed based on published methods.[60] Nanoparticles were seeded into individual wells containing DMEM and calf serum, and the absorbance at 650 nm was serially monitored at time 0, 1 week, and 2 weeks (Figure 3), with eight wells being inoculated under each of several conditions. Absorbance increased 2.2-fold over 2 weeks in DMEM containing calf serum alone. Because β-mercaptoethanol (BME) enhances the growth of certain microorganisms[66] and mammalian cells,[67] presumably owing to its antioxidant property, we evaluated the effect of low concentrations of this agent on the growth of nanoparticles. BME had a modest growth-promoting effect at 50 and 200 μM. The metabolic inhibitors antimycin A, sodium azide, and potassium cyanide significantly reduced the increase in absorbance, suggesting blockade of nanoparticle replication. Of the antibiotics tested, TCN (12 μg/mL) was the most effective, nearly preventing any increase in optical density (OD) 650 nm, whereas ampicillin (50 μg/mL) was of intermediate effectiveness. Gentamicin (15 μg/mL) and nalidixic acid (15 μg/mL) had no effect. These results were confirmed by visual inspection of plates. Our finding that TCN is maximally effective is in agreement with published findings[60] and suggests that patients receiving prolonged courses of TCN might have decreased nanoparticle loads. Therefore, nanoparticles appear to be sensitive to metabolic inhibitors, as well as specific antibiotics, including TCN.

WST-1 (4-[3-(4-iodophenyl)-2-(4-nitrophenyl)-2H-5-tetazolio]1,3-benzene disulphonate, Roche, Basel, Switzerland) is a replication indicator that can be used to monitor microbial growth[68] because respiratory reduction

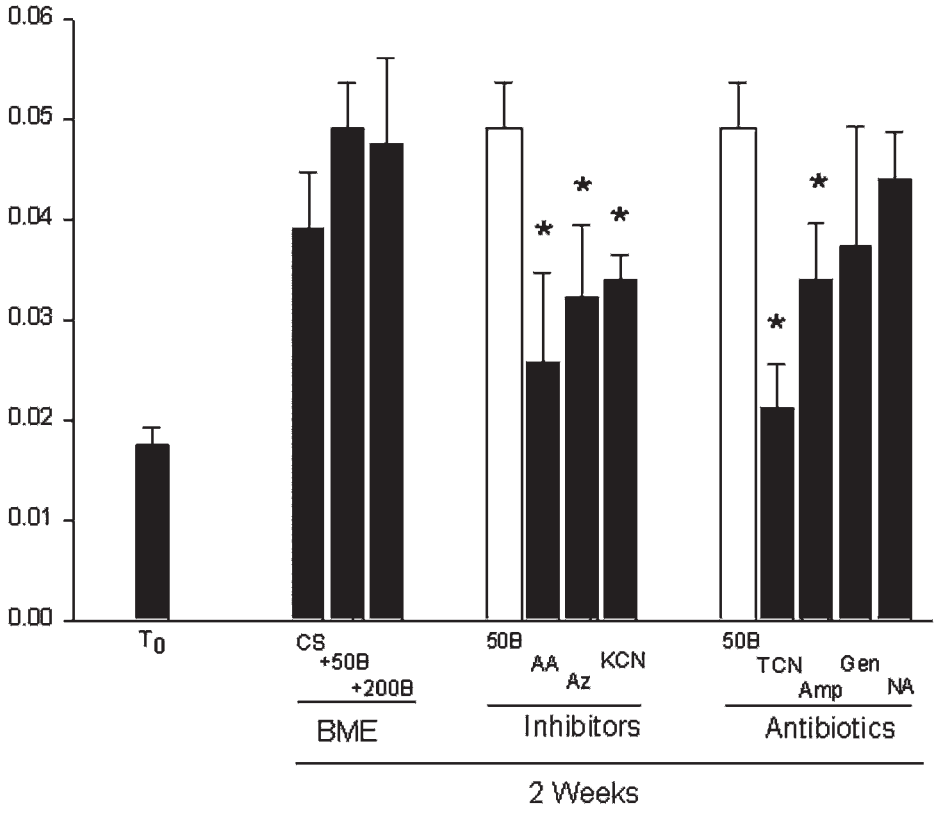

Figure 3 Effect of metabolic inhibitors and antibiotics on growth of nanoparticles. Nanoparticles were seeded into individual wells containing Dulbecco's Modified Eagle Medium (DMEM) and calf serum, and the absorbance at 650 nm was serially monitored at time 0 (T_0), 1 week, and 2 weeks. Absorbance increased 2.2-fold over 2 weeks in DMEM containing calf serum alone (CS). β-Mercaptoethanol (BME) had a modest growth-promoting effect at 50 and 200 mM compared with CS. The metabolic inhibitors antimycin A (AA), sodium azide (AZ), and potassium cyanide (KCN) significantly reduced the increase in absorbance, suggesting blockade of nanoparticle replication. Tetracyline (TCN) (12 μg/mL) nearly prevented an increase in optical density (OD) 650 nm, whereas ampicillin (Amp; 50 μg/mL) was of intermediate effectiveness, and gentamicin (Gen; 15 μg/mL) and nalidixic acid (NA; 15 μg/mL) had no effect. The results are expressed as mean ± standard error of measurement; $*p < .05$ versus control without inhibitors.

of this tetrazolium salt yields the colored compound formazan. Therefore, WST-1 can serve as an indicator of dehydrogenase activity as it shifts color on reduction by electrons flowing through the electron transport system, as well as by any superoxide radicals produced. When added to nanoparticle cultures in 96-well plates, increased WST-1 cleavage above background levels was observed at 24 but not 4 hours (Figure 4A). Enhanced conversion of WST-1 was observed in the presence of BME, with maximal effects at 100 μM (Figure 4B). Therefore, BME may enhance nanoparticle metabolism and growth initially, although after 2 weeks, only a minimal increase in cell number (as indicated by OD 650) was observed. Nanoparticles did not grow when flasks were placed in strictly anaerobic chambers (data not shown). Given that BME has been found to favor the growth of anaerobic as opposed to aerobic microorganisms,[66] it is possible that although nanoparticles are not strict anaerobes, nevertheless, they may be susceptible to oxidative stress. These data also suggest that BME may accelerate nanoparticle metabolism, at least transiently, and that WST-1 is useful to monitor nanoparticle metabolism.

Nanoparticle cultures have now been established from human kidney stones (16 of 32 submitted for elemental analysis), calcified human aortic aneurysms (8 of 9 obtained at the time of surgery), and aged (20 months) rat kidneys (2 of 2). Tissue samples were homogenized, filtered (0.2 μm), and inoculated into 10 mL of artificial urine. Kidney stone samples (50–100 mg) were pulverized, dissolved in 1 mL of 1 N HCl for 10 minutes, neutralized with an equal volume of 1 N NaOH, filtered, and inoculated into artificial urine. Visible growth occurred within 4 weeks. No growth was observed in control, uninnoculated cultures. Of particular importance, a calcified human aortic aneurysm that grew nanoparticles in culture revealed positive immunohistochemical staining with a monoclonal antibody directed against nanoparticles (8D10, obtained from Nanobac OY, Kuopio, Finland), whereas the aneurysm without growth in culture was negative by immunohistochemistry.[64] Nanoparticle isolates were scraped, pelleted, and fixed to glass slides (60°C × 15 minutes). Samples were then stained with a monoclonal antibody against nanoparticles (8D10, Nanobac OY) and counterstained with PicoGreen to localize DNA. Nanoparticle isolates obtained from human tissues have been recognized by this antibody and staining colocalized with PicoGreen DNA staining (Figure 5). Structures detected by immunofluorescence resembled the decalcified cells visualized by TEM (see Figure 3B). It is unlikely that these cultured organisms are common bacteria or *Chlamydia* because the samples were passed through a 0.2 μm filter at the time of initial culture, the incubation time (2–4 weeks) is

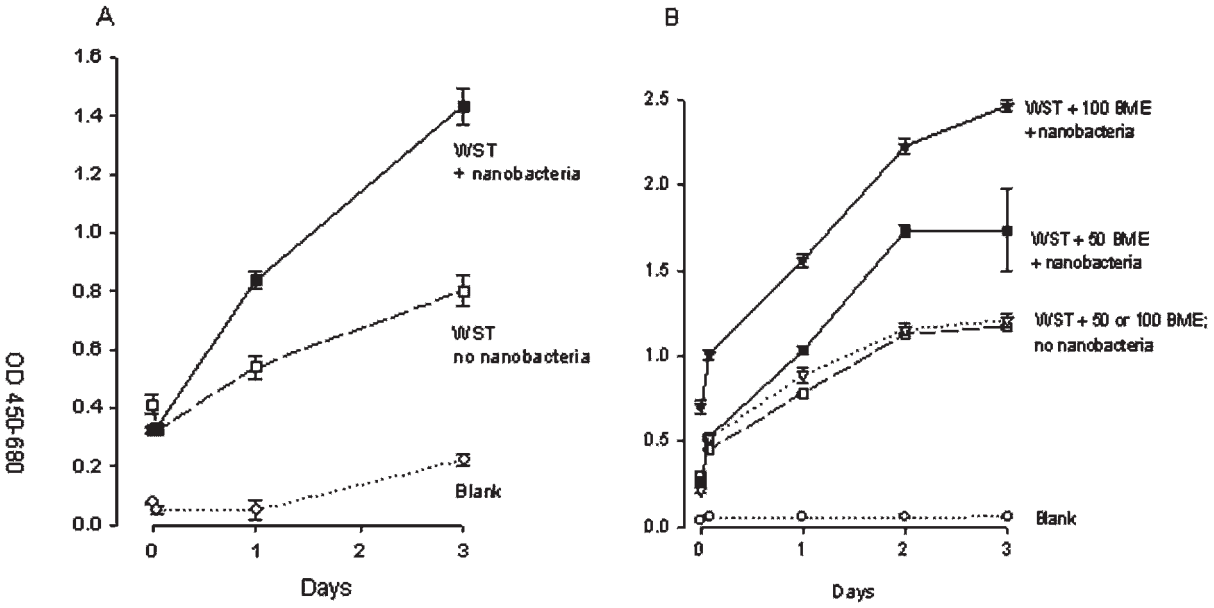

Figure 4 Quantification of nanoparticle growth using the replication indicator WST-1. *A*, When added to nanoparticle cultures in 96-well plates, increased WST-1 cleavage above background levels was observed at 24 but not 4 hours. *B*, Enhanced conversion of WST-1 was observed in the presence of β-mercaptoethanol (BME), with maximal effects at 100 μM. OD = optical density.

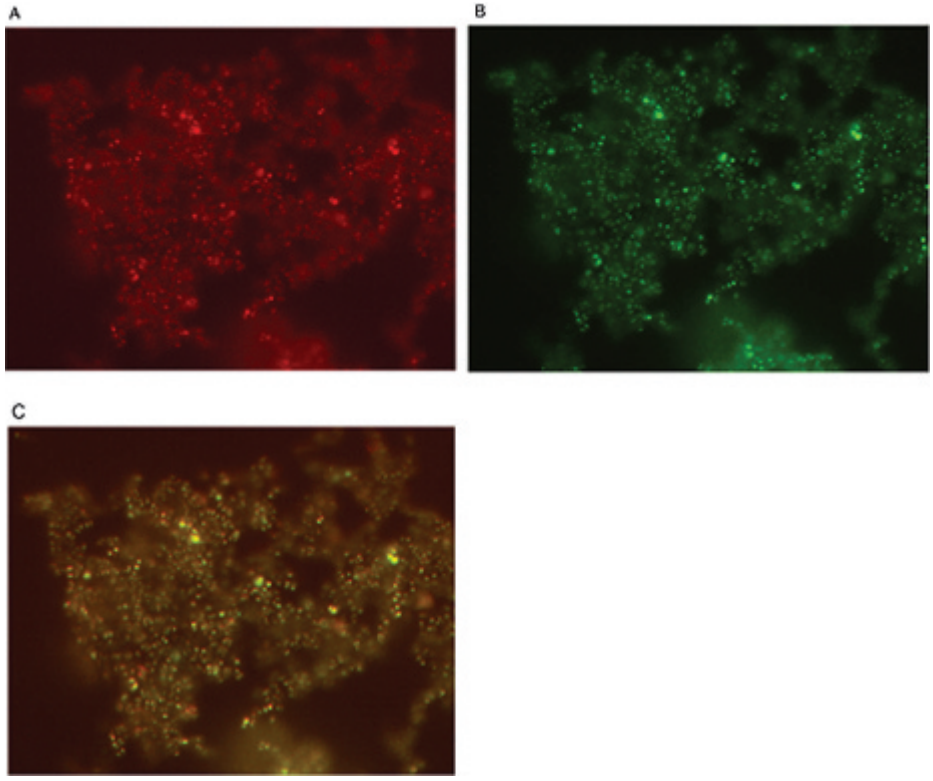

Figure 5 Nanoparticle isolate from a human calcium oxalate dihydrate (COD) kidney stone. Nanoparticles were concentrated by centrifugation and applied to a glass slide for staining. *A*, Positive immunofluorescence staining with antibody 8D10; *B*, DNA staining with PicoGreen; *C*, superimposition (×1,000 original magnification).

longer than common bacteria require, and the medium (in the absence of mammalian cells) does not support the growth of *Chlamydia*. Note that the size of a *Chlamydia* elementary body is ≈0.3 μm, whereas the reticulate body (reproductive form) is ≈1 μm. Our cultures were also negative for *Mycoplasma* when screened in the Mayo Clinical Microbiology Laboratory using a sensitive polymerase chain reaction–based test.

Next, nanoparticle proteins were characterized. Ten flasks each of nanoparticle strains S90 and NBCS were centrifuged, decalcified, and resolved by SDS-PAGE (Figure 6). A number of proteins were visualized, and the pattern of bands was similar for the two strains. A similar pattern of bands was seen in a protein lysate of nanoparticles isolated from human renal stones and recently published.[62] The most prominent S90 bands at 65 kDa and 45 kDa were submitted for mass spectrometry analysis, identifying them as elongation factor Tu (EF-Tu)[69] and GroEL,[70] respectively. EF-Tu is universally distributed among the three domains of life, displays considerable structural conservation, and is functionally constant, playing a role in the elongation of nascent polypeptides from the ribosome during translation.[69] Because of its highly conserved nature, EF-Tu has been employed extensively to investigate phylogenetic relationships.[71] GroEL is another conserved chaperoning protein found in prokaryotes that mediates adenosine triphosphate–dependent protein folding of cytosolic proteins to prevent their aggregation.[70,72] Analysis of a third band at 70 kDa revealed two proteins, dihydrolipoamide acetyltransferase of pyruvate dehydrogenase and polyribonucleotide nucleotidyl transferase. Pyruvate dehydrogenase is an important enzyme in the citric acid cycle and branched-chain amino acid metabolism, whereas in prokaryotes, polynucleotide phosphorylase can both synthesize RNA by using nucleotide diphosphates as precursors and exonucleolytically degrade RNA in the presence of inorganic phosphate. The latter enzyme has an important function, adding the polyadenylated tail to messenger RNA.[73] By mass spectroscopy, fragments from all four proteins matched most closely to proteins derived from prokaryotes (as opposed to eukaryotes such as the cow, as might be expected if the proteins were derived from calf serum). Therefore, nanoparticles contain numerous proteins, which is not unexpected for a living microorganism. In

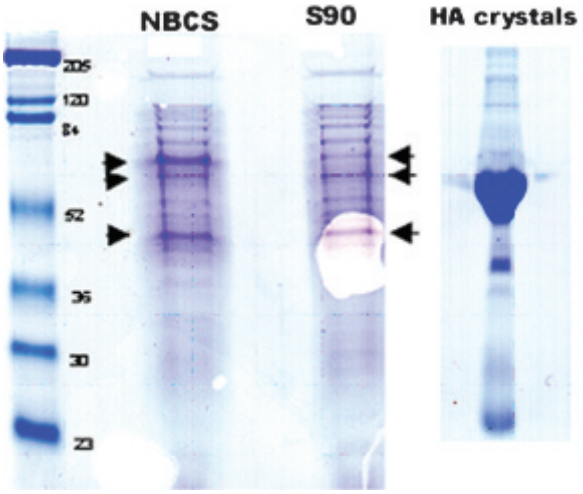

Figure 6 Nanoparticle proteins. Nanoparticle strains "S90" and "NBCS" and inorganic hydroxyapatite (HA) crystals incubated in Dulbecco's Modified Eagle Medium and calf serum were decalcified, solubilized in gel loading buffer, and subjected to sodium dodecyl sulfate–polyacrylamide gel electrophoresis. Prominent bands at 45 kDa (elongation factor Tu), 65 kDa (GroEL), and 70 kDa (dihydrolipoamide acetyltransferase of pyruvate dehydrogenase and polyribonucleotide nucleotidyl transferase) were identified by mass spectrometry analysis in the Mayo Clinic Protein Core Facility. HA crystals, unlike nanoparticles, bind large quantities of albumin.

addition, when inorganic hydroxyapatite crystals were incubated with DMEM containing 10% calf serum for 1 week, rinsed, and then dissolved, a vastly different array of proteins was visualized, including a predominant band at ≈67 kDa (presumably bovine serum albumin). Therefore, the array of proteins isolated from nanoparticles seems unlikely to have been nonspecifically derived from serum contaminants.

Because of the small size and calcium phosphate shell, traditional methods for extraction of nucleic acids from nanoparticles have not been effective. Using a simplified protocol used to isolate DNA from the cultures of archeae that employs pretreatment with proteinase K,[74] we have now successfully and reproducibly identified a strong and single ≈25 kB basepair band of DNA in the nanoparticle cultures (Figure 7). Ten flasks containing nanoparticle strain S90 were scraped, centrifuged, and decalcified in EDTA (200 μL, 0.5 M, pH 8.0) overnight at 4°C. The pellet was gently sonicated (4 × 10 seconds at 5 μm) and untreated (see Figure 7A) or treated with proteinase K (100 μg/mL overnight at 50°C) (see Figure 7B). Proteinase K was inactivated by treatment at 80°C × 5 minutes, and 10% of the sample was resolved by gel electrophoresis. Without proteinase K treatment, the sample did not enter the gel (see Figure 7A), whereas a band, apparently 25 kB, was clearly

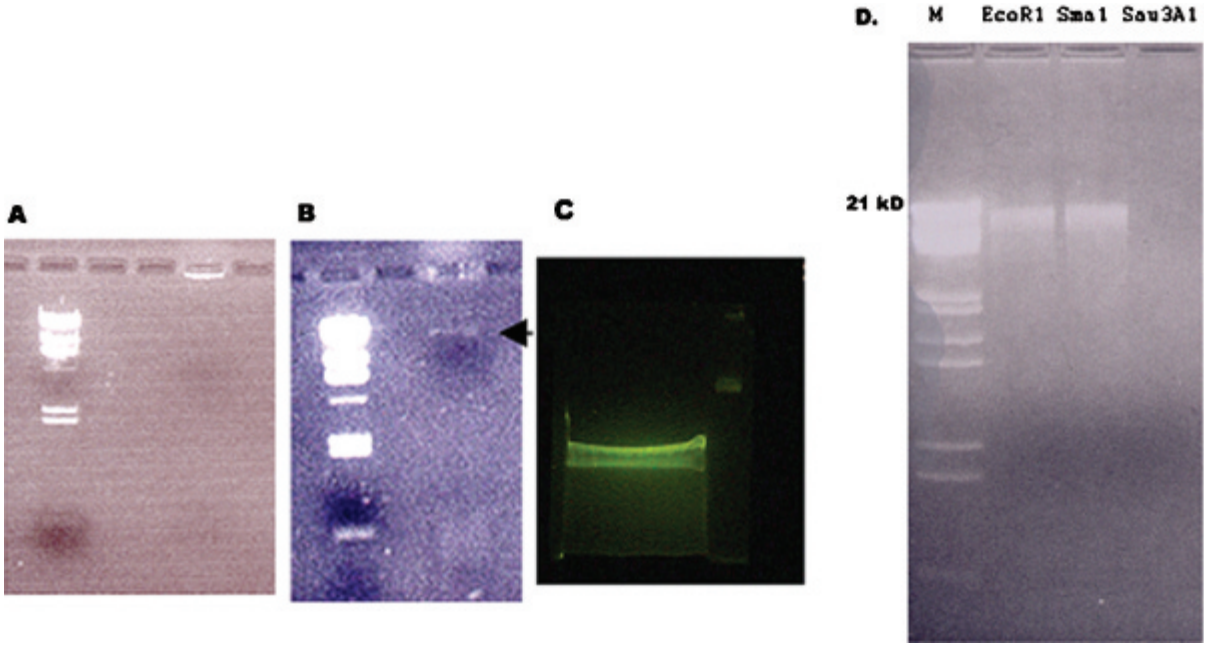

Figure 7 Nanoparticle deoxyribonucleic acid (DNA). When treated with proteinase K, nanoparticle DNA entered a 1% gel (*arrow, B*), whereas untreated DNA did not (*A*). A large quantity of DNA was loaded onto a low–melting point gel for further purification in *C*. This band was digested by the four-basepair cutting endonuclease SauI3A1 into a diffuse smear of 0 to 500 base pairs (*D, far right*). The six-basepair endonucleases EcoR1 and Sma1 did not reduce the apparent size of the band (*D*).

visualized by ethidium bromide staining after proteinase K digestion (see Figure 7B, arrow). It is not clear if this band represents the entire genome or is a fragment, such as a plasmid. Often additional DNA is left within the wells. Nevertheless, isolation of a single band has been extremely consistent in each batch of nanoparticles processed using this protocol to date. A larger amount of DNA was subsequently prepared from 50 flasks, treated with proteinase K, loaded onto a low–melting point gel and stained with SYBRGold (Molecular Probes; see Figure 7C). It is likely that the nanoparticle DNA band is actually quite larger than 25 kB because on a 0.4% gel, it still ran with the size of the largest molecular-weight marker (> 50 kB). We demonstrated that this band is cleaved by the endonuclease Sau3A1 and transformed into a diffuse smear (see Figure 7C; 0–500 bp).

Attempts are ongoing to obtain a unique sequence from this DNA material. However, our initial experiments do support the existence of self-replicating particles of 50 to 100 nm in size that appear to contain DNA. Are they a true life form or an example of inorganic biomineralization? Much work remains.

Conclusions

Interstitial Randall's plaques appear to represent the precursor of the majority of idiopathic calcium oxalate stones, the most common variety. Yet the nature of the evolution remains unknown. In this article, we reviewed three possible mechanisms of their formation: transcytosis of crystals from the tubular lumen, direct nucleation in the interstitium, perhaps driven by secretion of osteoblast-like proteins, or colonization by a novel, self-replicating, calcifying entity. These three possibilities might not be mutually exclusive. For example, cell injury can promote expression of crystal-binding molecules or transition of an epithelial cell to an osteoblast-like phenotype (Figure 8). At this point, the role of nanoparticles in

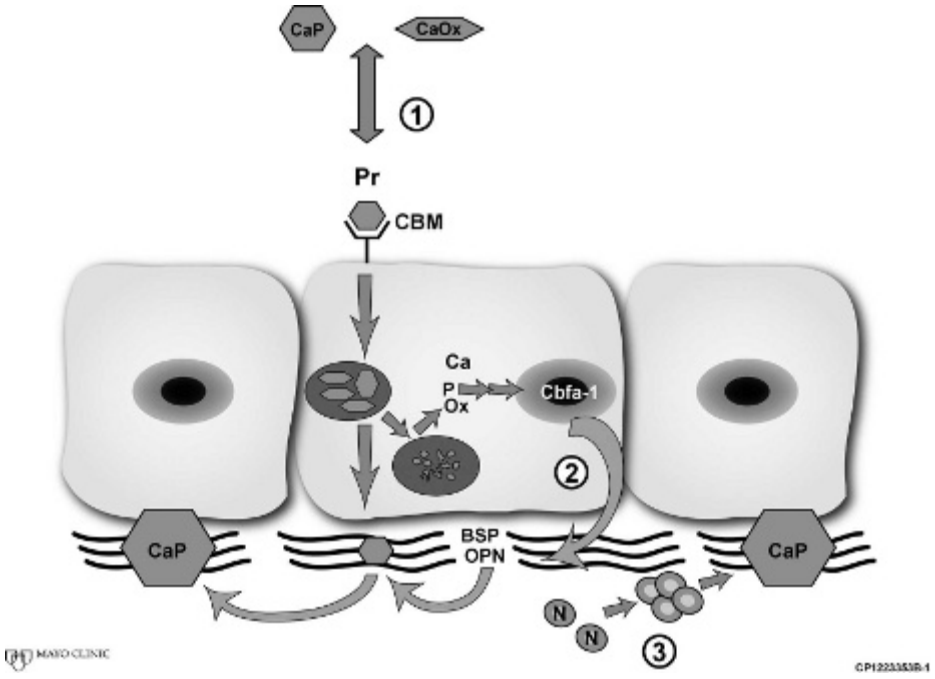

Figure 8 Potential pathways to produce a Randall's plaque. CaOx or CaP crystals that form in tubular fluid could bind to tubular cells (*pathway 1*). Potential crystal-binding molecules (CBM) include hyaluronan and annexin II, and both appear to be expressed on the apical surface only in response to injury or stress. Once adherent, crystals can be internalized within vesicles. Urinary protein inhibitors (Pr) within luminal fluid can block nucleation, growth, or aggregation of crystals or their adhesion to renal cells. Once inside cells, crystals could be transcytosed to the interstitium or dissolve, releasing Ca, Ox, and P. The presence of Pr within crystal or crystal aggregates can facilitate their dissolution within cells. Ions released by dissolving crystals or other secondary signals could trigger transcription factors that could, in turn, lead to secretion of matrix proteins, including bone sialoprotein (BSP) and osteopontin (OPN), which could promote interstitial nucleation of crystals (*pathway 2*). Alternatively, nanoparticles (N) could colonize the interstitium, perhaps owing to a favorable metabolic milieu, and perhaps stimulate renal cell transformation to a bone cell phenotype (*pathway 3*).

these events is entirely speculative, albeit intriguing. Our studies do provide evidence that these controversial entities can be propagated in vitro and contain conserved bacterial proteins and DNA. An important goal would be to obtain a unique genetic signature or to allow definitive clinical investigation in disease states such as nephrolithiasis.

Whatever the pathophysiologic steps in the evolution of Randall's plaques and renal stones, it seems unlikely that these events are driven solely by physical chemistry but rather are critically influenced by proteins and cells, and understanding these events will provide clues toward novel therapeutic targets.

Acknowledgments

We thank Jon Butz of the Mayo Clinic Metals Laboratory for determination of intracellular calcium and Joanne Zimmerman for excellent secretarial assistance.

References

1. Unwin R, Wrong O, Cohen E, et al. Unraveling of the molecular mechanisms of kidney stones. Lancet 1996;348: 1561–5.
2. National Kidney and Urological Diseases Advisory Board 1990 long range plan: window on the 21st century. J Urol 1991;145:S68–93.
3. Randall A. The origin and growth of renal calculi. Ann Surg 1937;105:1009–20.
4. Randall A. Papillary pathology as precursor of primary renal calculus. J Urol 1940;44:580–9.
5. Cifuentes Delatte L, Minon-Cifuentes J, Medina JA. New studies on papillary renal calculi. J Urol 1987;137:1024–9.
6. Stoller ML, Low RK, Shami GS, et al. High resolution radiography of cadaveric kidneys: unraveling the mystery of Randall's plaque formation. J Urol 1996;156:1263–6.
7. Low RK, Stoller ML. Endoscopic mapping of renal papillae for Randall's plaques in patients with urinary stone disease. J Urol 1997;158:2062–4.
8. Evan AP, Lingeman JE, Coe FL, et al. Randall's plaque of patients with nephrolithiasis begins in basement membranes of thin loops of Henle. J Clin Invest 2003;111:602–5.
9. Robertson WG, Peacock M, Nordin BEC. Calcium oxalate crystalluria and urine saturation in recurrent renal stone formers. Clin Sci 1971;40:365–74.
10. Dent CE, Sutor DJ. Presence or absence of inhibitor of calcium-oxalate crystal growth in urine of normals and of stone-formers. Lancet 1971;1:776–8.
11. Robertson WG, Peacock M, Marshall RW, et al. Saturation-inhibition index as a measure of the risk of calcium oxalate stone formation in the urinary tract. N Engl J Med 1976;294:249–52.
12. Felix R, Monod A, Broge L, et al. Aggregation of calcium oxalate crystals: effect of urine and various inhibitors. Urol Res 1977;5:21–8.
13. Lieske JC, Norris R, Swift H, Toback FG. Adhesion, internalization and metabolism of calcium oxalate monohydrate crystals by renal epithelial cells. Kidney Int 1997;52: 1291–301.
14. Lieske JC, Norris R, Toback FG. Adhesion of hydroxyapatite crystals to anionic sites on the surface of renal epithelial cells. Am J Physiol 1997;273:F224–33.
15. Kumar V, Farell G, Lieske JC. Whole urinary proteins coat calcium oxalate monohydrate crystals to greatly decrease their adhesion to renal cells. J Urol 2003;170:221–5.
16. Chauvet MC, Ryall RL. Intracrystalline proteins and calcium oxalate crystal degradation in MDCK II cells. J Struct Biol 2005;151:12–7.
17. Scurr DS, Robertson WG. Modifiers of calcium oxalate crystallization found in urine. III. Studies on the role of Tamm-Horsfall mucoprotein and of ionic strength. J Urol 1986;136:505–7.
18. Hess B, Nakagawa Y, Coe FL. A new spectrophotometric method for measuring calcium oxalate monohydrate crystal aggregation in the absence of supersaturation: inhibitory effects of urinary glycoproteins. Urol Res 1989;17:149–50.
19. Grover PK, Moritz RL, Simpson RJ, Ryall RL. Inhibition of growth and aggregation of calcium oxalate crystals in vitro—a comparison of four human proteins. Eur J Biochem 1998;253:637–44.
20. Asplin JR, Arsenault D, Parks JH, et al. Contribution of human uropontin to inhibition of calcium oxalate crystallization. Kidney Int 1998;53:194–9.
21. Enghild JJ, Thorgersen IB, Cheng F, et al. Organization of the inter-alpha-inhibitor heavy chains on the chondroitin sulfate originating from ser10 of bikunin: posttranslational modification of IaI-derived bikunin. Biochemistry 1999;38: 11804–13.
22. Stapleton AMF, Ryall RL. Crystal matrix protein: getting blood out of a stone. Miner Electrolyte Metab 1994;20: 299–309.
23. Hess B, Nakagawa Y, Parks JH, Coe FL. Molecular abnormality of Tamm-Horsfall glycoprotein in calcium oxalate nephrolithiasis. Am J Physiol 1991;260:F569–78.
24. Knörle R, Schnierle P, Koch A, et al. Tamm-Horsfall glycoprotein: role in inhibition and promotion of renal calcium oxalate stone formation studied with Fourier-transform infrared spectroscopy. Clin Chem 1994;40:1739–43.
25. Schnierle P. A simple diagnostic method for the differentiation of Tamm-Horsfall glycoproteins from healthy probands and those from recurrent calcium oxalate renal stone formers. Experientia 1995;51:1068–72.
26. Jefferson A, Reynolds TM, Elves A, Wierzbicki AS. Patients with recurrent renal stones have a physico-chemically altered urinary Tamm-Horsfall glycoprotein profile. Ann Clin Biochem 1996;33(Pt 6):540–4.
27. Durrbaum D, Rodgers AL, Sturrock ED. A study of crystal amtrix extract and urinary prothrombin fragment 1 from a stone prone and stone free population. Urol Res 2001;29: 83–8.
28. Kumar V, Pena de la Vega L, Farell G, Lieske JC. Urinary macromolecular inhibition of crystal adhesion to renal

epithelial cells is impaired in male stone formers. Kidney Int 2005;68:1784–92.
29. Mo L, Huang HY, Zhu XH, et al. Tamm-Horsfall protein is a critical renal defense factor protecting against calcium oxalate crystal formation. Kidney Int 2004;66:1159–66.
30. Wesson JA, Johnson RJ, Mazzali M, et al. Osteopontin is a critical inhibitor of calcium oxalate crystal formation and retention in renal tubules. J Am Soc Nephrol 2003;14:139–47.
31. Sumitra K, Pragasam V, Sakthivel R, et al. Beneficial effect of vitamin E supplementation on the biochemical and kinetic properties of Tamm-Horsfall glycoprotein in hypertensive and hyperoxaluric patients. Nephrol Dial Transplant 2005;20:1407–15.
32. Lieske JC, Leonard R, Swift HS, Toback FG. Adhesion of calcium oxalate monohydrate crystals to anionic sites on the surface of renal epithelial cells. Am J Physiol 1996;270: F192–9.
33. Bigelow MW, Wiessner JH, Kleinman JG, Mandel NS. Surface exposure of phosphatidylserine increases calcium oxalate crystal attachment. Am J Physiol 1997;272:F55–62.
34. Yamate T, Kohri K, Umekawa T, et al. Osteopontin antisense oligonucleotide inhibits adhesion of calcium oxalate crystals in Madin-Darby canine kidney cell. J Urol 1999;160:1506–12.
35. Sorokina EA, Kleinman JG. Cloning and preliminary characterization of a calcium-binding protein closely related to nucleolin on the apical surface of inner medullary collecting duct cells. J Biol Chem 1999;274:27491–6.
36. Verkoelen CF, Van Der Boom BG, Romijn JC. Identification of hyaluronan as a crystal-binding molecule at the surface of migrating and proliferating MDCK cells. Kidney Int 2000;58:1045–54.
37. Kumar V, Farell G, Deganello S, Lieske JC. Annexin II is present on renal epithelial cells and binds calcium oxalate monohydrate crystals. J Am Soc Nephrol 2003;14:289–97.
38. Farell G, Huang E, Kim SY, et al. Modulation of proliferating renal epithelial cell affinity for calcium oxalate monohydrate crystals. J Am Soc Nephrol 2004;15:3052–62.
39. Lieske JC, Spargo B, Toback FG. Endocytosis of calcium oxalate crystals and proliferation of renal tubular epithelial cells in a patient with type 1 primary hyperoxaluria. J Urol 1992;148:1517–9.
40. Saxon A, Busch GJ, Merrill JP, et al. Renal transplantation in primary hyperoxaluria. Arch Intern Med 1974;133:464–7.
41. Mandell I, Krauss E, Millan JC. Oxalate-induced acute renal failure in Crohn's disease. Am J Med 1980;69:628–32.
42. Wharton R, D'Agati V, Magun AM, et al. Acute deterioration of renal function associated with enteric hyperoxaluria. Clin Nephrol 1990;34:116–21.
43. Gelbart DR, Brewer LL, Fajardo LF, Weinstein AB. Oxalosis and chronic renal failure after intestinal bypass. Arch Intern Med 1977;137:239–43.
44. Hering F, Briellmann T, Luoend G, et al. Stone formation in the human kidney. Urol Res 1987;15:67–73.
45. Gonlusen G, Akgun H, Ertan A, et al. Renal failure and nephrocalcinosis associated with oral sodium phosphate bowel cleansing: clinical patterns and renal biopsy findings. Arch Pathol Lab Med 2006;130:101–6.
46. Carr G, Simmons NL, Sayer JA. Disruption of clc-5 leads to a redistribution of annexin A2 and promotes calcium crystal agglomeration in collecting duct epithelial cells. Cell Mol Life Sci 2006;63:367–77.
47. Verhulst A, Asselman M, De Naeyer S, et al. Preconditioning of the distal tubular epithelium of the human kidney precedes nephrocalcinosis. Kidney Int 2005; 68:1643–7.
48. Chen NX, Moe SM. Vascular calcification in chronic kidney disease. Semin Nephrol 2004;24:61–8.
49. Bostrom K, Watson KE, Horn S, et al. Bone morphogenetic protein expression in human atherosclerotic lesions. J Clin Invest 1993;91:1800–9.
50. Fitzpatrick LA, Severson A, Edwards WD, Ingram RT. Diffuse calcification in human coronary arteries. Association of osteopontin with atherosclerosis. J Clin Invest 1994;94: 1597–604.
51. Shanahan CM, Cary NR, Salisbury JR, et al. Medial localization of mineralization-regulating proteins in association with Monckeberg's sclerosis: evidence for smooth muscle cell-mediated vascular calcification. Circulation 1999;100:63–8.
52. Shanahan CM, Cary NR, Metcalfe JC, Weissberg PL. High expression of genes for calcification-regulating proteins in human atherosclerotic plaques. J Clin Invest 1994;93:2393–402.
53. Kleinman JG, Sorokina EA. Cloning and preliminary characterization of a calcium-binding protein closely related to nucleolin on the apical surface of inner medullary collecting duct cells. J Biol Chem 1999;274:27941–6.
54. Wada T, McKee MD, Steitz S, Giachelli CM. Calcification of vascular smooth muscle cell cultures: inhibition by osteopontin. Circ Res 1999;84:166–78.
55. Kajander EO, Kuronen I, Akerman K, et al. Nanobacteria from blood, the smallest culturable autonomously replicating agent on earth. Proc SPIE 1997;3111:420–8.
56. Ciftcioglu N, Pelttari A, Kajander EO. Extraordinary growth phases of nanobacteria isolated from mammalian blood. Proc SPIE 1997 3111, 429–35.
57. Hjelle JT, Miller-Hjelle MA, Poxton IR, et al. Endotoxin and nanobacteria in polycystic kidney disease. Kidney Int 2000;57:2360–74.
58. Akerman KK, Kuikka JT, Ciftcioglu N, et al. Radiolabeling and in vivo distribution of nanobacteria in rabbit. Proc SPIE 1997;3111:436–42.
59. Ciftcioglu N, Bjorklund M, Kuorikoski K, et al. Nanobacteria: an infectious cause for kidney stone formation. Kidney Int 1999;56:1893–8.
60. Ciftcioglu N, Miller-Hjelle MA, Hjelle JT, Kajander EO. Inhibition of nanobacteria by antimicrobial drugs as measured by a modified microdilution method. Antimicrob Agents Chemother 2002;46:2077–86.
61. Khullar M, Sharma SK, Singh SK, et al. Morphological and immunological characteristics of nanobacteria from human renal stones of a north Indian population. Urol Res 2004; 32:190–5.

62. Cisar JO, Xu D-Q, Thompson J, et al. An alternative interpretation of nanobacteria-induced biomineralization. Proc Natl Acad Sci U S A 2000;97:11511–5.
63. Kim K. Calcification of matrix vesicles in human aortic valve and aortic media. Fed Proc 1976;35:156–62.
64. Miller VM, Rodgers G, Charlesworth JA, et al. Evidence of nanobacterial-like structures in calcified human arteries and cardiac valves. Am J Physiol Heart Circ Physiol 2004;287: H1115–24.
65. Kajander EO, Ciftcioglu N. Nanobacteria: an alternative mechanism for pathogenic intra- and extracellular calcification and stone formation. Proc Natl Acad Sci U S A 1998; 95:8274–9.
66. Mattern KL, Evans CA, Lara JC. Selective antibacterial action of 2-mercaptoethanol on propionobacteria in skin cultures. Appl Environ Microbiol 1979;37:177–9.
67. Inui K, Oreffo ROC, Triffit JT. Effects of beta mercaptoethanol on the proliferation and differentiation of human osteoprogenitor cells. Cell Biol Int 1997;21:419–25.
68. Johnsen AR, Bendixen K, Karlson U. Detection of microbial growth on polycyclic aromatic hydrocarbons in microtiter plates by using the respiration indicator WST-1. Appl Environ Microbiol 2002;68:2683–9.
69. Jenkins C, Fuerst JA. Phylogenetic analysis of evolutionary relationships of the planctomycete division of the domain bacteria based on amino acid sequences of elongation factor Tu. J Mol Evol 2001;52:405–18.
70. Chaudhuri TK, Farr GW, Fenton WA, et al. GroEL/GroES-mediated folding of a protein too large to be encapsulated. Cell 2001;107:235–46.
71. Baldauf SL, Palmer JD, Doolittle WF. The root of the universal tree and the origin of eukaryotes based on elongation factor phylogeny. Proc Natl Acad Sci U S A 1996;93: 7749–54.
72. Weissman JS. The ins and outs of GroEL-mediated protein folding. Mol Cell 2001;8:730–2.
73. Mohanty BK, Kushner SR. Polynucleotide phosphorylase functions both as a 3′ right arrow 5′ exonuclease and a poly(A) polymerase in Escherichia coli. Proc Natl Acad Sci U S A 2000;97:11966–71.
74. Baumann C, Judex M, Huber H, Wirth R. Estimation of genome sizes of hyperthermophiles. Extremophiles 1998;2: 101–8.